Geomechanics and Engineering, *Vol. 26, No. 5 (2021) 415-425*
https://doi.org/10.12989/gae.2021.26.5.415

Seismic earth pressure on embankment gravity retaining wall with nonuniform slope

Honglue Qu*, Yuanyuan Deng[a], Qindi Hu[b], Xue Huang[c] and Chenxu Wang[d]

School of Geoscience and Technology, Southwest Petroleum University, No. 8, Xindu Avenue, Xindu District, Chengdu, Sichuan, China

(Received October 24, 2020, Revised June 29, 2021, Accepted August 3, 2021)

Abstract. According to the results of a survey of retaining structures damaged by the Wenchuan earthquake, the damage to gravity retaining walls accounted for 97.1% of the total damage to retaining walls. Among gravity retaining structures, embankment gravity retaining walls with nonuniform slopes are more prone to be disturbed under seismic conditions. However, relatively few studies have been performed to calculate the seismic earth pressure on such structures. In this study, a simplified approach is presented to calculate the seismic earth pressure on embankment gravity retaining walls with nonuniform slopes. In the proposed approach, the equations are derived based on the primary assumptions of the Mononobe–Okabe theory and the limit equilibrium state of the quadrilateral slip soil wedge. To verify the applicability of the proposed approach, a large-scale shaking-table test was conducted to obtain the distribution of the seismic earth pressure, the magnitude of earth pressure resultant force, the resultant force action point, and slip surface of an embankment gravity retaining wall with a nonuniform slope, under various peak ground accelerations. A comparison indicates that the calculated results were in agreement with the experimental results, implying that the proposed approach is valid for calculating the seismic earth pressure on embankment gravity retaining walls with nonuniform slopes.

Keywords: embankment gravity retaining wall with nonuniform slope; peak ground acceleration; seismic earth pressure; shaking-table test

1. Introduction

The gravity retaining wall (GRW) is the most commonly used type of retaining wall because of its simple form, easily obtainable construction materials, and convenient construction. However, according to the results of the survey of damage caused to a retaining structure in the Wenchuan earthquake, the GRW is most vulnerable to seismic damage(Zhang *et al.* 2012). Thus, seismic earth pressure on the GRW has become a significant topic that is being investigated by several scholars (Santhoshkumar and Ghosh 2018; Jesmani *et al.* 2016). Steedman and Zeng (1990) studied the seismic earth pressure based on the pseudo-dynamic Mononobe–Okabe method. Choudhury and Nimbalkar (2007) used the pseudo-dynamic method to analyse the active and passive earth pressures behind the retaining wall; they improved the method too. Sitar *et al.* (2012) completed an experimental program to evaluate seismically induced earth pressures on different types of retaining structures. Wagner *et al.* (2018) calculated the resultant force of seismic earth pressure on a rigid wall using pseudo-static limit equilibrium methods and elastic wave equation analyses. Jo *et al.* (2017) used the pseudo-static method to calculate the dynamic earth pressure based on force equilibrium using the Mononobe–Okabe extension of Coulomb's earth pressure theory. Among the numerous previous research studies on this topic, most have focused on the shoulder-type gravity retaining wall that is as high as the backfill (Yang and Li 2018; Chowdhury and Singh 2015). In practical engineering, the form of the GRW connected to the road through the embankment with the top of the wall lower than the backfill with nonuniform slope is also common. So far, there have been several studies on the static response of the embankment gravity retaining wall with a nonuniform slope (EGWNS) (Ma *et al.* 2014; Zhang *et al.* 2011). However, there has been little research on the dynamic response of the EGWNS under seismic conditions. For this type of EGWNS, Coulomb's earth pressure theory can be used to calculate the earth pressure. However, this theory is only applicable to cases in which the backfill surface is inclined. Culmann's graphical method, based on Coulomb's earth pressure theory, can be used to calculate the earth pressure when the ground is irregular; however, this method involves a large number of calculations and drawing work and is not accurate. Okabe (1926) and Mononobe and Matsuo (1929) proposed the classical *Mononobe–Okabe* method (M-O method) to calculate the seismic earth pressure based on the Coulomb theory by using the pseudo-static method. The seminal experiments were performed by Mononobe and Matsuo (1929) using a

*Corresponding author, Associate Professor
E-mail: geoqhl@126.com
[a]Master Student
E-mail: dengyuanyuanly@163.com
[b]Undergraduate Student
E-mail: huqindihuxiyao@163.com
[c]Master Student
E-mail: geoyhx@163.com
[d]Master Student
E-mail: wangcx003@126.com

ISSN: 2005-307X (Print), 2092-6219 (Online)

shaking table. The mechanical principle of the M-O method is clear; the results obtained were consistent with the measured results. Since then, numerous 1*g* shaking-table experiments have been conducted by several researchers, including Matsuo (1941), Matsuo and Ohara (1960), Bolton and Steedman (1982), and Ishibashi and Fang (1987). Mikola *et al.* (2016) performed a series of centrifuge experiments on model retaining and basement structures with medium dense cohesionless backfill, the maximum dynamic earth pressures obtained increase with depth and can be reasonably approximated by a triangular distribution analogous to that used to represent static earth pressures. In general, the results of these studies were in agreement with the original results obtained by Mononobe *et al.* (1929) and Okabe (1926).

Based on previous studies, we establish a theoretical calculation model and present a simplified calculation approach derived from the M-O method to calculate the seismic earth pressure on the EGWNS. This model breaks through the limitation of the M-O method, which cannot be used when the backfill has a nonuniform slope, and simplifies the formula for the calculation of seismic earth pressure. Thereafter, the test model is established considering seismic conditions to verify the applicability of the proposed approach. The Wenchuan earthquake wave is selected as the input wave to conduct the large-scale shaking-table test, and the seismic earth pressure distribution, magnitude of earth pressure resultant force, and location of the point of action of seismic earth pressure resultant force of the EGWNS are selected as parameters for comparison. A comparison with the calculated results indicates good agreement, which implies that the proposed approach is applicable and provides a reliable basis for the seismic design of the EGWNS. The results of this study are compared with those of scholars based on seismic design codes of different countries, and seismic design parameters are proposed for the EGWNS with the aim of reducing the degree of damage to it under seismic conditions.

2. Simplified calculation approach

Considering seismic active earth pressure, for example, and using cohesionless soil as the backfill behind the rigid EGWNS (Cilingir *et al.* 2011), the theoretical model of the proposed approach was established, as illustrated in Fig. 1. The Coulomb earth pressure theory is used in the proposed approach, assuming that the backfill behind the wall slides down along the back of the wall and a certain plane of the backfill to form an arbitrary quadrilateral slip soil wedge shape; the slip soil wedge can easily reach the limit equilibrium state. The seismic active earth pressure on the EGWNS can be obtained based on the force system equilibrium condition of the arbitrary quadrilateral slip soil wedge.

Fig. 1 depicts the calculation diagram of theoretical model, where G is the weight of the soil wedge ABCD, the slip surface BC is assumed to be an inclined plane, R is the reaction force of the soil on the slip surface BC, and the angle between R and the normal to the slip surface BC is

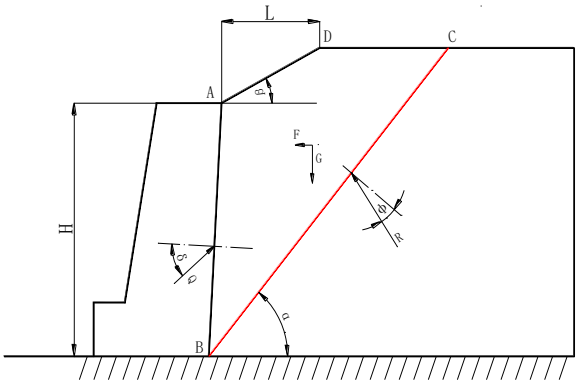

Fig. 1 Calculation diagram of theoretical model

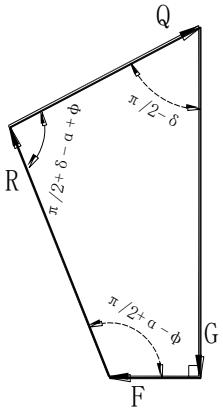

Fig. 2 Slip soil wedge force system equilibrium diagram

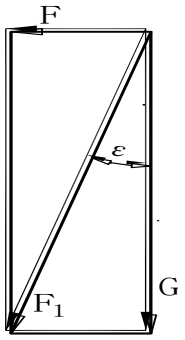

Fig. 3 Synthetic diagram of seismic inertia force and slip soil wedge weight

equal to the internal friction angle φ of the backfill. Q is the force exerted by the retaining wall on the soil wedge, and the angle between Q and the normal to the back of the wall is equal to the friction angle δ between the back of the wall and the backfill. L is the horizontal projection length of the slope, β is the angle between the slope and the horizontal plane, H is the height of the retaining wall, and α is the angle between the slip surface BC and the ground surface. Considering the static equilibrium condition of the slip soil wedge body ABCD, a closed force quadrilateral consisting of four forces G, R, Q, and F (seismic inertia force) is illustrated in Fig. 2. It should be noted that the retaining wall structure generally has a strong resistance to vertical loads and a weak resistance to horizontal forces.

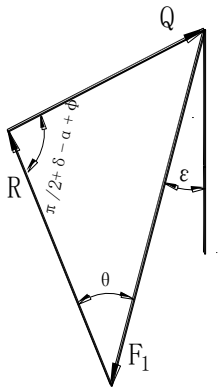

Fig. 4 Simplified diagram of the force equilibrium of the slip soil wedge

Therefore, horizontal ground motion should be considered; hence, in this study, we only consider horizontal earthquakes.

To simplify the calculation, the forces F and G are synthesised to obtain the resultant force F_1, as depicted in the synthetic diagram presented in Fig. 3, where ε is the seismic angle between F_1 and G.

Similarly, based on the static equilibrium conditions, a closed force triangle was formed by the three forces Q, R, and F_1, as illustrated in Fig. 4, where θ is the angle between R and F_1 obtained as $\theta = \varepsilon + \alpha - \varphi$.

Therefore, according to the sine theorem:

$$\frac{F_1}{\sin\left(\frac{\pi}{2}+\delta-\alpha+\varphi\right)}=\frac{Q}{\sin\theta} \tag{1}$$

Eq. (1) could be rewritten as:

$$Q=\frac{\gamma H^2\sin\theta\cos\alpha}{2\sin\alpha\cos\varepsilon\cos(\varphi+\delta-\alpha)}+\frac{\gamma L^2\sin\theta\tan\beta^2}{2\tan\alpha\cos\varepsilon\cos(\varphi+\delta-\alpha)}-\frac{\gamma L^2\sin\theta\tan\beta}{2\cos\varepsilon\cos(\varphi+\delta-\alpha)} \tag{2}$$

If the peak ground acceleration (PGA) is known, the seismic angle ε can be calculated using the standard formula $\varepsilon=\tan^{-1}\left(\mu A_g/g\right)$, where μ is the comprehensive seismic influence coefficient, which is determined according to the region, attenuation characteristics of earthquake motion and site conditions. Chinese researchers have determined the value of the comprehensive seismic influence coefficient(μ) through a large number of engineering experiments, when calculating the seismic angle, the values of μ for soil foundation and rock foundation are 0.25 and 0.2 respectively(GB 50330-2013). In this paper, μ=0.25 is the empirical value obtained by previous researchers defined in the reference specification and A_g is the peak ground motion acceleration.

Therefore, Q changes only with the inclination α of the sliding surface BC. It will have a maximum value Q_{max} corresponding to the active earth pressure E_a. To calculate the value of Q_{max}, the expression for α was derived from Eq. (2), and $dQ/d\alpha$ was set equal to 0 ($dQ/d\alpha=0$). Thus, we have

$$\left[\gamma\left(H^2+L^2\tan\beta^2\right)\tan(\varphi+\delta)\sin^2\alpha-\gamma L^2\tan\beta^2\right]\tan^2\alpha+\gamma L^2\tan\beta^2\tan(\varphi+\delta)\tan\alpha-\gamma\left(H^2+L^2\tan\beta^2\right)\cos^2\alpha\tan\alpha+\gamma\left(H^2+L^2\tan\beta^2\right)\tan(\varphi+\delta)=0 \tag{3}$$

As all the parameters used in Eq. (3) are known in the case of engineering design, the value of α can be obtained and substituted into Eq. (2) using the Mathematica software. Thus, the Coulomb active earth pressure can be obtained as $E_a = Q_{max}$.

For the safety and economy consideration of an embankment gravity retaining wall with a nonuniform slope design, according to Technical code for building slope engineering (GB 50330-2013), the wall height of soil slope should not exceed 10m. In Eq. (2), it is necessary to satisfy $\varphi+\delta-\alpha<\frac{\pi}{2}$, and the range of β can be set according to the properties of different fillers.

3. Sensitivity analysis on the slope angle and the length of the flat part of the slope

Since the standard sand is used in the shaking table test,

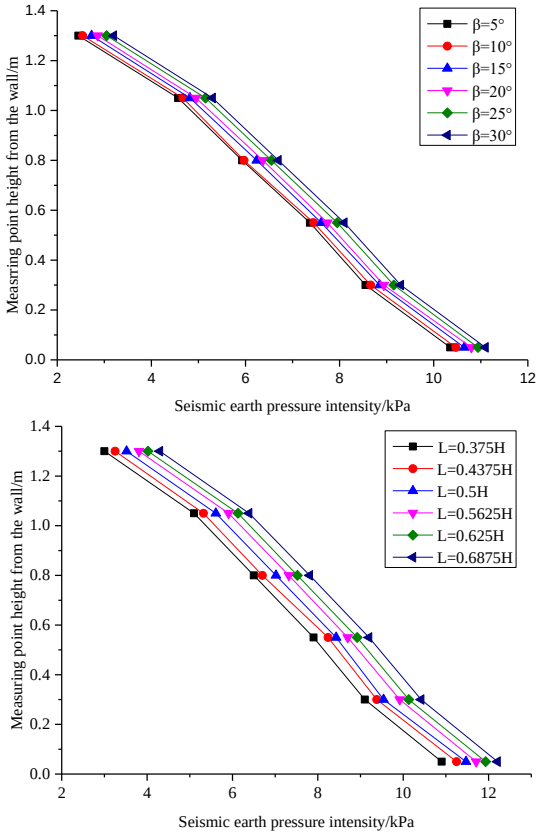

Fig. 5 Sensitivity analysis of seismic earth pressure intensity under different slope angle and different length of the flat part of the slope

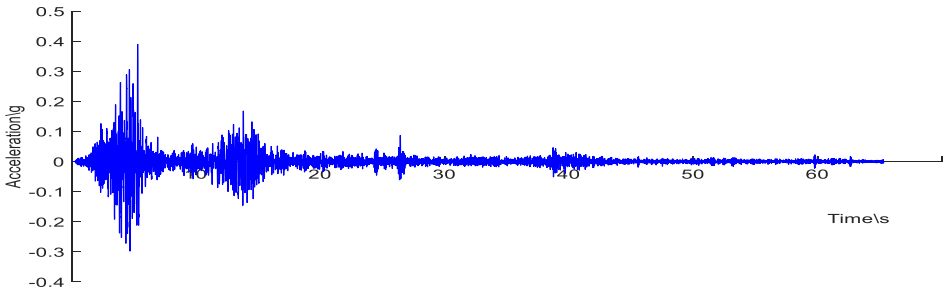

Fig. 6 The acceleration time history of compressed PGA=0.4 g

the characteristics of the fill behind the wall of the theoretical model are consistent with the standard sand. The natural angle of repose (the limit angle of slope formed by sand accumulation under natural stable state, called natural angle of repose) of standard sand is equal to or close to its internal friction angle. Within the range of natural angle of repose, the single factor sensitivity analysis (only one factor in the calculation model is changed to a certain extent each time, and other factors remain unchanged) is carried out on the slope angle(β) and the length of the flat part of the slope(L) of EGWNS. Ensure that other factors remain unchanged, take β = 5°, 10°, 15°, 20°, 25° and 30° to calculate the corresponding seismic earth pressure; similarly, take L = 0.375H, 0.4375H, 0.5H, 0.5625H, 0.625H, 0.6875H to calculate the corresponding seismic earth pressure, as shown in Fig. 5. It can be seen from Fig. 5 that within the natural angle of repose, with the increase of β, the seismic earth pressure intensity gradually increases, the difference is not obvious. The seismic earth pressure intensity increases by 0.19kPa for every 5 ° increase of β; With the increase of L, the seismic earth pressure intensity gradually increases, too. But the difference is relatively obvious, the seismic earth pressure intensity increases by 0.29 kPa for every 0.0625H increase of L. Through the above analysis, it can be seen that the influence of L is greater than β, so the influence of the length of the flat part of the slope is more sensitive. More attention should be paid to the length of the flat part of the slope for guiding the design and reinforcement of retaining walls.

4. Experimental validation

4.1 Test facilities

The shaking-table test was conducted on a large-scale, high-performance seismic simulation test platform in the Nuclear Power Research and Design Institute of China. The shaking table has dimensions of 6 m × 6 m, the ability to move along six degrees of freedom, a maximum loading weight of 600 kN, a maximum horizontal displacement of ±150 mm, and a maximum vertical displacement of ±100 mm. The horizontal and vertical maximum accelerations under the full loading condition are 1 *g* and 8 *g*, respectively. The corresponding horizontal and vertical maximum accelerations for the unloading condition are 3 *g* and 2.6 *g*, respectively, and the frequency range is 0.1–80 Hz. The PGAs of the Wenchuan Wolong wave in the *X*-direction were selected as the input waves for the shaking-table test. The selected waves were scaled according to a similarity time compression ratio of 1:2.45, and the input motion duration was set as 65.3 s, as depicted in Fig. 6. The following values were used for the PGAs of the seismic waves: 0.1 *g*, 0.2 *g*, 0.4 *g*, 0.7 *g*, 0.9 *g*. During the shaking-table test, a 128-channel base band modem (BBM) data acquisition system was used, with the maximum referenced error being less than or equal to 0.5%. A signal adapter was connected with a charge converter to convert the voltage signals, with the maximum reference error being less than or equal to 1%. Data acquisition, signal monitoring, and online analysis were performed synchronously.

Table 1 Similitude relationships of the test model

Parameters	Dimension	Similitude relationship	Similitude ratio
Length L	L	λ	6
Density	ML^{-3}	λ_ρ	1
Acceleration $\ddot{u}$	LT^{-2}	λ_{ii}	1
Speed $\dot{u}$	LT^{-1}	$\lambda^{1/2}$	2.45
Displacement u	L	λ	6
Time t	T	$\lambda^{1/2}$	2.45
Frequency ω	T^{-1}	$\lambda^{-1/2}$	0.408
Stress σ	FL^{-2}	$\lambda_\sigma = \lambda_\rho \lambda$	6
Force F	F	$\lambda_F = \lambda_\sigma \cdot \lambda^2$	6^3

4.2 Similitude relationship in experimental model

The reliability of the model test is determined by the similarity of the test model and prototype. Harris (1982), one of the early scholars in this field, explored and studied the model's dynamic similarity theory based on the shaking table, which laid a foundation for the development of the test technology for the structural model. In this paper, based on the Buckingham π theorem (Evans and John 1972) and dimensional analysis method, by considering the stress-strain constitutive relationship between the model and the prototype, the design similarity constant of the test model of the retaining wall is obtained. In the similitude design, the geometric dimension L, mass density ρ, and seismic acceleration a are selected as the fundamental quantities with the similitude constants of C_L=6, $C\rho$ =1, and C_a=1, respectively (Qu *et al.* 2016) and the similarity constants of the physical quantities are presented in Table 1. Because the

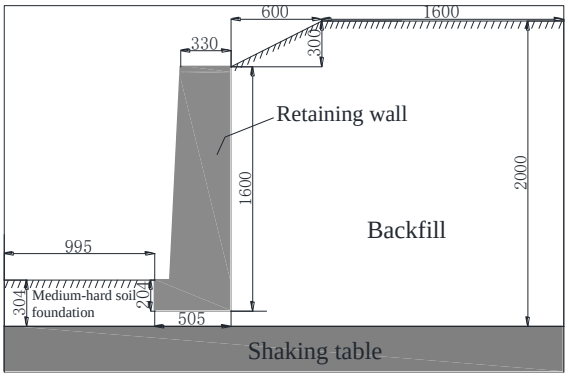

Fig. 7 Design of the experimental model (unit: *mm*)

Fig. 8 Shaking table test model

mechanical properties of subgrade filling are very complex, and its nonlinear characteristics begin to appear when the strain level is low, so it is impossible to achieve the complete similarity between the prototype and the model in the dynamic situation. Therefore, in view of this shortcoming, the standard sand filling of layered compaction is used as the simulation material of subgrade in this experiment, and the similarity between the prototype and the model is deduced based on the shear strength similarity theory, which is also the most commonly used method at present (Xu *et al.* 2020).

4.3 Construction of experimental model

This experiment simulates the dynamic response characteristics of the EGWNS with a height of 9.6 m. The size of the experimental model based on the geometric similarity ratio is depicted in Fig. 7. The slope is divided into two sections. At the starting point of the slope located at the top of the wall, the horizontal and vertical projection lengths are 0.6 and 0.3 m, respectively; in the second section, these values are 1.6 and 0 m, respectively. The length and depth of the backfill in front of the wall are 0.995 m and 0.305 m, respectively. The length and depth of the backfill behind the wall are 2.2 m and 2 m, respectively. The experimental models are illustrated in Figs. 7 and 8.

4.4 Soil

Standard sand (natural quartz sea sand with $SiO_2 > 96\%$)

Table 2 Soil properties of the backfill and foundation

	USCS classification	Sand (%)	e_{max} [a]	e_{min} [b]	φ(°) [c]	c(kPa) [d]	Relative density(%)
Backfill	SP	96	0.96	0.61	33	-	72
Foundation	SW	86	0.76	0.57	30.4	6.9	81

[a] Max void ratios
[b] Min void ratios
[c] Internal friction angle
[d] Cohesion force

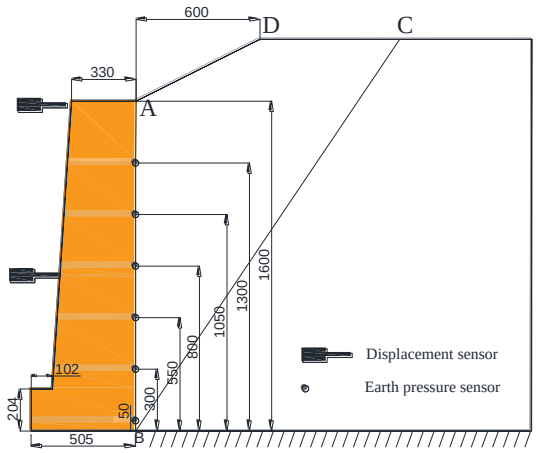

Fig. 9 Installation of the displacement and earth pressure sensors (unit: *mm*)

Table 3 Final displacement of the EGWNS

PGA	Displacement of the wall top (mm)	Wall rotation angle (°)	Displacement indexes
A_g/g	Δ_1 [a]	η	$\Delta 1/H$
0.1	0	0.0000	0.00%
0.2	0.1052	0.0029	0.01%
0.4	6.6914	0.1988	0.42%
0.7	56.14729	1.6930	3.51%
0.8	90.25108	2.8804	5.64%

[a] Δ_1 include both sliding and rotational displacements

is used as the backfill material to simulate the prototype, and materials similar to undisturbed soil, such as kaolin, bentonite, and gelatin particles, are used to simulate the medium–hard soil foundation (Kagawa *et al.* 2004). Table 2 presents the soil properties of the backfill and foundation. The model parameters are obtained through physical tests, such as direct shear, water content, pycnometer test method and consolidated drained triaxial tests (CD triaxial tests). The unit weight of the backfill is 17 kN/m^3. According to the roughness of the back of the wall and the drainage condition, the friction angle δ between the back of the wall and the backfill is set as 0.5φ. The unit weight of the foundation is 20.26 kN/m^3, and the water content is 3.6%. It should be noted that the low cohesion, 6.92 kPa, used for the test foundation is decided based on the similitude design of the scaled shake-table test model. The relative density of backfill and foundation soil is 72% and 81% respectively by pycnometer test method. The results of the CD triaxial tests

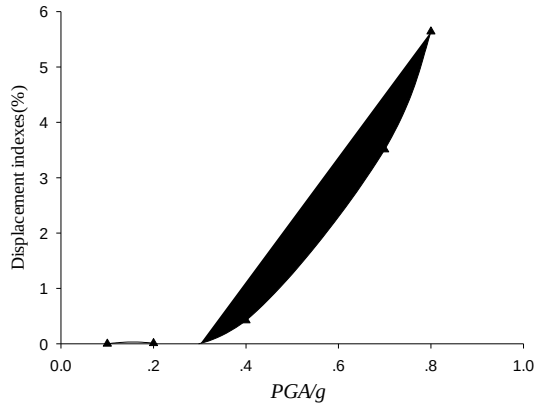

Fig.10 The displacement indexes in different PGA values

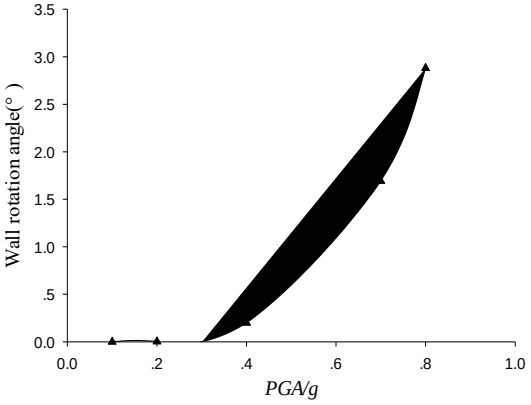

Fig.11 The wall rotation angle in different PGA values

indicate that as the confining pressure increases, the relationship between the stress and strain exhibits a significant dilatation phenomenon, and the peak stress increases with the increase in confining pressure. The large area in the middle of the filling is compacted in layers using small vibrating table machinery, and the model boundary is constructed via manual compaction.

4.5 Measuring point layout

The back of the wall is concrete and rough, and it is assumed that there is no relative slip between the backfill and the retaining wall. A series strain-type earth pressure box is selected as the earth pressure sensor; it can accurately measure the stress on soil, mud, and sand in or around the model. The sensor uses a strained full-bridge circuit to accurately eliminate the effect of temperature changes on the instrument. This test uses the YB-12 model with the smallest diameter among all models in the series; the sensor diameter is 12 mm; the thickness is 4.2 mm; the accuracy error is less than or equal to 0.3F-S; the overload capacity is 120%; and the bridge resistance is 350 Ω. To measure the intensity of earth pressure at different wall heights, six strain-type earth pressure sensors were arranged at 0.05, 0.30, 0.55, 0.80, 1.05, and 1.3 m, respectively, from the bottom of the wall contacting the backfill. The range of measurement of the displacement sensor is 5 cm with a measurement accuracy of 0.001 mm; two displacement sensors were arranged at the wall to measure its displacement. The arrangement of the earth pressure and displacement sensors is depicted in Fig. 9.

4.6 Monitoring record of wall displacement

The displacements of the wall under various loading conditions were recorded in the experiment. The total displacement, wall rotation angle, and displacement indexes (the displacement index is defined as the ratio of the total displacement of the top of the wall to the wall height, which comprehensively reflects the displacement amplitude of the wall after seismic activity) under different loading conditions are presented in Table 3. The diagram of displacement indexes and the wall rotation angle for different PGA values are depicted in Figs. 10-11, respectively.

It can be seen from Table 3 that the displacement of the top of the wall and the wall rotation angle increase with increase in the seismic intensity, and the magnitude of the displacement of the top of the wall increases differently under various seismic intensities. When the PGA is smaller than 0.4 g, the displacement of the wall is very small; the wall displacement indexes at 0.1*g* and 0.2*g* are also small and can be ignored. When the PGA is higher than or equal to 0.4*g*, the magnitude of the displacement of the top of the wall increases further with increase in the PGA. These results are consistent with those of Mikola *et al.*'s study (2016), in which they examined the deflections of the displacing retaining wall with a flat backfill.

5. Comparison of experimental and calculated results

5.1 Analysis of intensity of earth pressure

In the process of preparing for shaking table test, because the retaining wall is built first and then filled with backfill, the whole retaining wall inevitably has a certain displacement in the filling process. Through field measurement, the displacements in Translation modes(T) and Rotation about base modes(RB) are about 0.5231mm and 0.8734mm, respectively, both of which exceed the displacement value required to reach the active earth pressure state(Sherif *et al.* 1982). With the earth pressure sensors installed, the time history curve of the intensity of seismic earth pressure at different heights of the back of the wall can be measured, taking the peak value for safety as the comparison object at that location; thus, the distribution of the intensity of seismic earth pressure along the wall can be obtained. The measured and calculated intensities of seismic earth pressure were compared when the input PGAs were 0.1*g*, 0.2*g*, 0.4*g*, 0.7*g*, and 0.9*g* (Qu *et al.* 2018). The diagrams depicting the comparisons are presented in Figs. 12(a)-12(e), respectively.

Based on the comparison between the measured and calculated results, the following conclusions were drawn:

• The general trends in the intensities of seismic earth

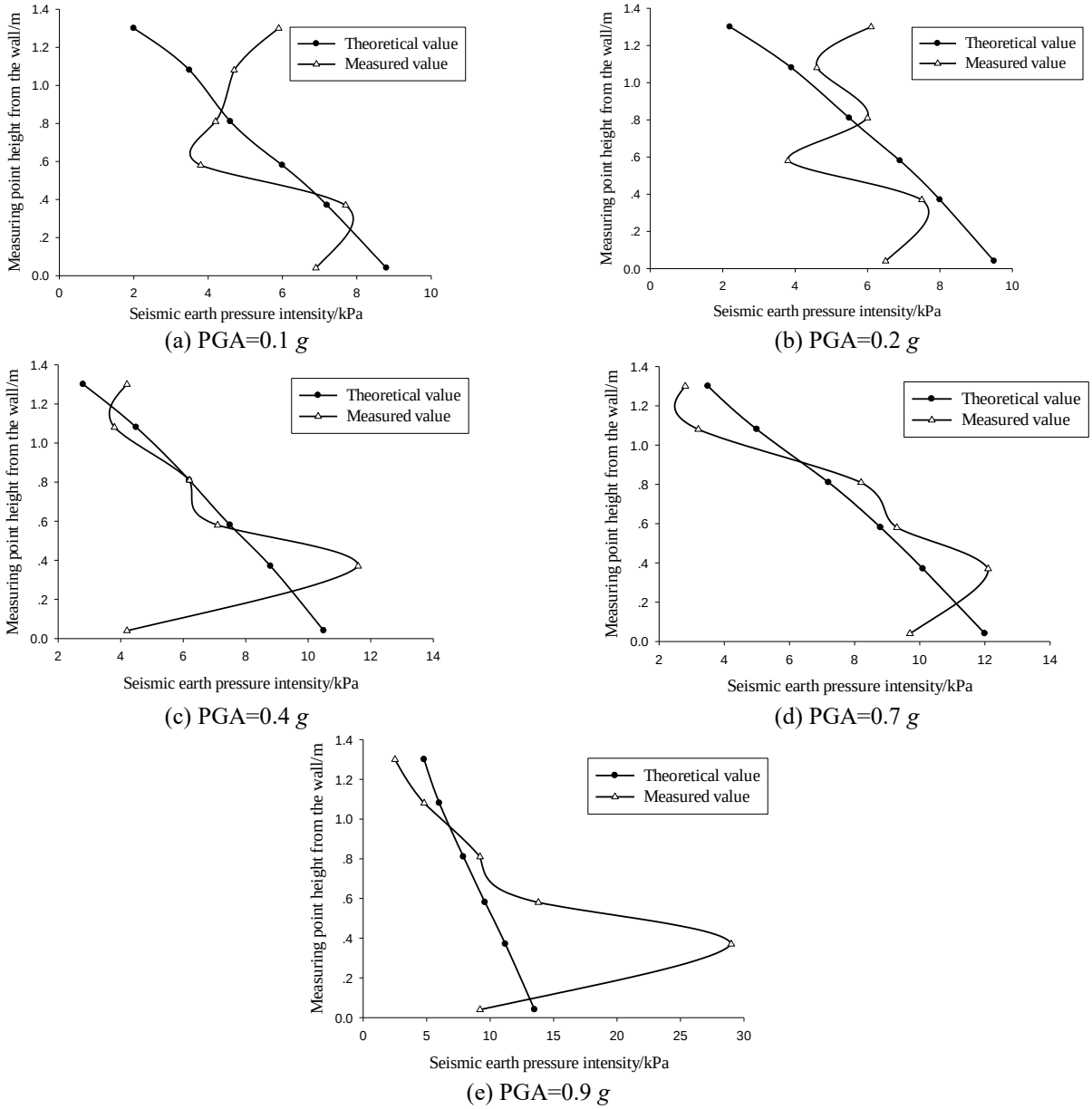

(a) PGA=0.1 *g* (b) PGA=0.2 *g*

(c) PGA=0.4 *g* (d) PGA=0.7 *g*

(e) PGA=0.9 *g*

Fig. 12 Comparison of measured and calculated of seismic earth pressure intensity in different PGA values

pressure obtained by calculation and measurement are similar—they increase gradually from the top of the wall to the bottom. The intensity of seismic earth pressure calculated using the proposed approach presents a triangular distribution; the intensity increases linearly with the increase in PGA. This is consistent with the results obtained using the M-O method and Mylonakis *et al.*'s (2007) method. However, the measured intensity of seismic earth pressure presents a nonlinear distribution. The intensity changes slowly at the top of the EGWNS and rapidly at the bottom. The reason for this difference may be the displacement of the wall under seismic conditions and the fact that the wall is fixed in the X-direction, which causes the curvature in the diagram of the intensity of seismic pressure. However, the effect of the displacement of the wall was not considered in the theoretical calculation.

• The maximum values of the calculated intensity of seismic earth pressure always appear at the bottom of the EGWNS. The peak values of the measured intensity of seismic earth pressure always appear near H/8–H/5 from the bottom of the wall, which are inconsistent with the findings of the M-O theory. Under the conditions of low seismic intensity (when the seismic intensity is below 8 degree, the maximum intensity occurs approximately at H/8 from the bottom of the wall; under high seismic intensity conditions (i.e., when the seismic intensity is higher than or equal to 8 degrees), the maximum intensity occurs approximately at H/5 from the bottom of the wall. When the PGA is lower than 0.4g, the maximum values of the calculated intensity are higher than those of the measured intensity, and when the PGA is higher than or equal to 0.4 g, the maximum values of the measured intensity are higher than those of the calculated intensity.

• When the PGA is lower than 0.4 g, the measured values of the intensity of seismic earth pressure near the bottom of the wall at H/5 are lower than the calculated

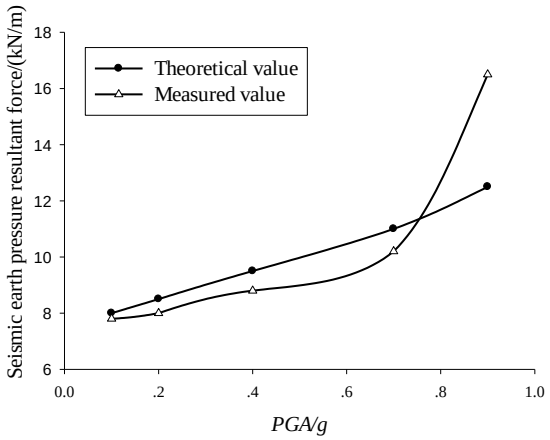

Fig. 13 Comparison diagram of seismic earth pressure

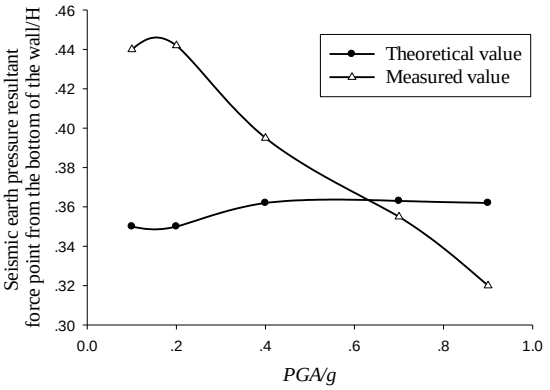

Fig. 15 Seismic earth pressure resultant point from the bottom of the wall

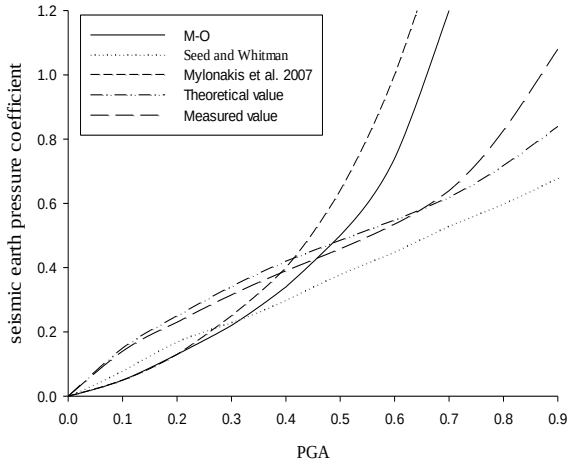

Fig. 14 Comparison of seismic earth pressure coefficient under different PGAs obtained by different methods

values. With the increase in PGA, the curve of the measured intensity of seismic earth pressure indicates increasingly evident external convexity. There are two reasons for this phenomenon: first, there is high residual stress (After the load action stops, the influence of the load action on the retaining wall cannot disappear completely, but there is still some residual in the retaining wall, then the influence and action of the residual is called residual stress) near the bottom of the wall. And the area under residual stress increases with the increase in PGA. When the PGA is lower than 0.4 g, the increase in the area under residual stress with the increase in PGA is not significant. However, when the PGA exceeds 0.4 g, the area under residual stress expands rapidly with the increase in PGA. The second is that the previous shakes in the experimental process will affect the experimental data. However, the displacement of the wall in each stage of the test is small, we can simply think that the influence of the previous shakes on the peak value of the seismic earth pressure is relatively small, that is, the influence on the increment of earth pressure intensity at the measuring point is not significant.

5.2 Comparison analysis of seismic earth pressure

After the intensity of seismic earth pressure is measured by each sensor, the area enclosed by the distribution curve and the coordinate axis can be calculated to obtain the seismic earth pressure resultant force. Similarly, the theoretically calculated seismic earth pressure resultant force can be obtained. A comparison is presented in Fig. 13. It can be seen from the figure that the measured and calculated values of the seismic earth pressure are roughly proportional to the PGA; in addition, the higher the PGA is, the more the seismic earth pressure increases. When A_g = 0.1 g, the difference in seismic earth pressure between the two results was 4.8% and when A_g = 0.2 g, 0.4 g, 0.7 g, and 0.9 g, the differences were 4.7%, 7.4%, 6.9%, and 26.7%, respectively. Thus, it can be seen that the differences between the two results are related to the PGA. When the PGA is lower than 0.4 g, the relative displacement between the bottom of the wall and the backfill is very small. With the PGA increases and reaches 0.7 g, the backfill reaches the shear strength and plastic deformation occurs, which is the main reason for the large difference between the two curves depicted in Fig. 13 beyond PGA = 0.7 g.

Furthermore, the method proposed in this study is compared with those proposed in previous studies that have used the seismic earth pressure coefficient based on different national seismic design codes, such as M-O theory based on Japanese codes and Mylonakis' results based on European codes, as depicted in Fig. 14. The comparison indicates that the trend in the theoretical value of the seismic earth pressure coefficient is roughly the same as that identified in previous studies, and that the value increases with the increase in the PGA. The M-O method provides amply conservative results over the full range of accelerations, whereas the method proposed in this study avoids overdesign while ensuring safety. In addition, the earth pressure coefficient of the earthquake defined by the M-O method increases exponentially beyond 0.6 g, which indicates that the M-O formula is not applicable to high-intensity areas. Moreover, the trend in the experimental values is observed to be very similar to that in the theoretical values, further verifying the accuracy of the proposed method.

5.3 Comparison of point of action of seismic earth pressure resultant

The point of action of the seismic earth pressure

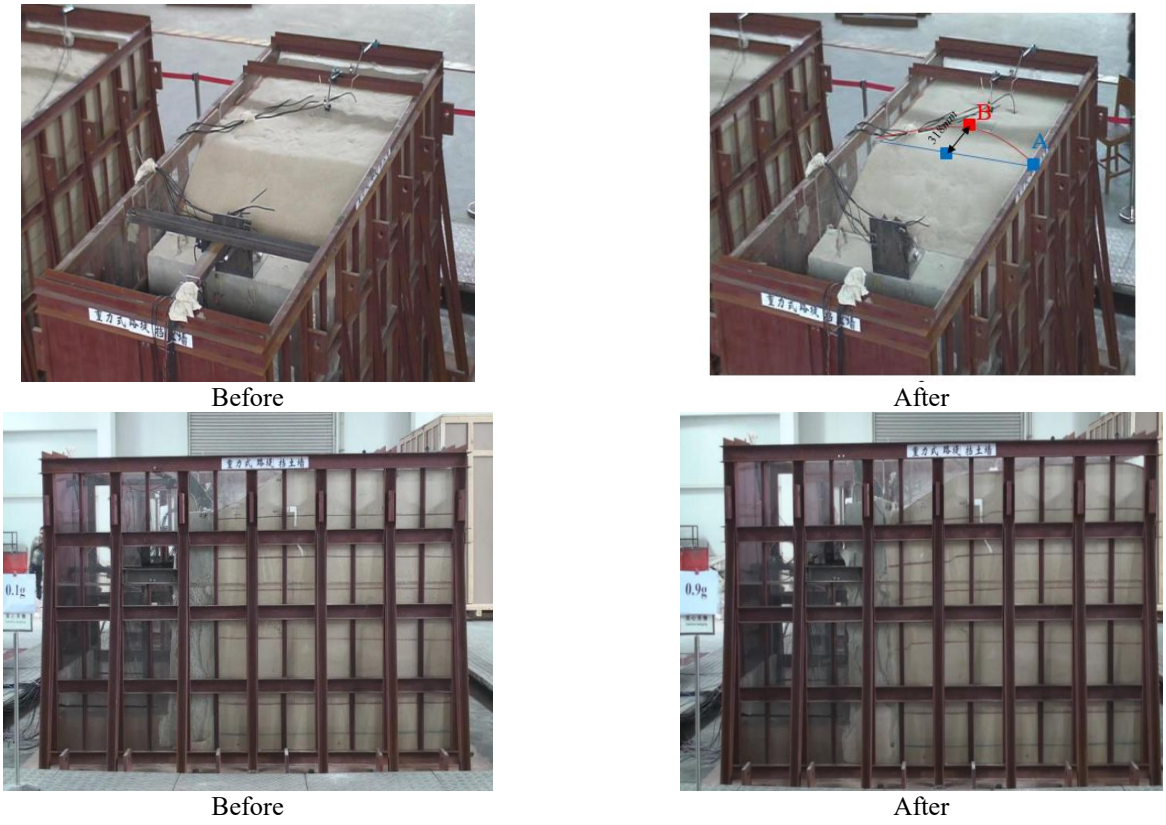

Fig. 16 The diagrams of shaking table test

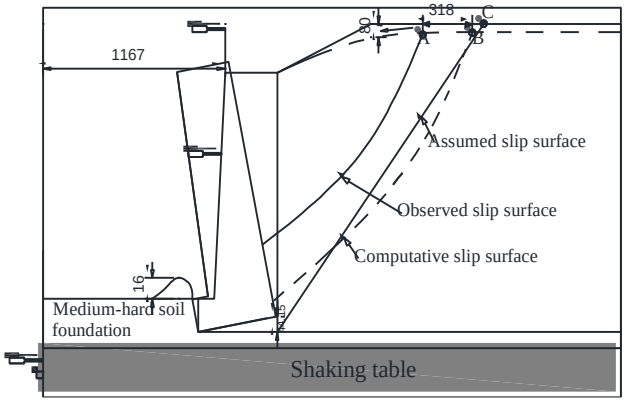

Fig. 17 Comparison diagram of the slip surface under PGA=0.9 g (unit: *mm*)

resultant can be obtained through the geometric heights of the measured and calculated seismic earth pressure intensities, as depicted in Fig. 15.

It can be seen from the figure that the measured point decreases with the increase in PGA and the calculated point increases with the increase in PGA. The calculated results indicate that the resultant force point is higher than 0.33*H*, as specified by the M-O formula and the modified M-O method proposed by Mylonakis *et al.* (2007) at different PGAs. The measured results indicate that the resultant force point is higher than 0.33*H*, as specified by the M-O formula, only when the PGA is low; with the increase in PGA, the resultant force point gradually decreases to 0.33*H*, as specified by the M-O formula. The main reasons for these phenomena are as follows: (1) the increase in PGA leads to an increase in the displacement of the top of the wall and a larger area of residual stress in the lower part of the retaining wall; the intensity of seismic earth pressure in the lower part of the wall increases significantly too. (2) The rotation and displacement of the wall causes the subgrade filling to subside relative to the top of the wall. (3) The increase in the displacement of the wall causes the shear strength of the backfill to weaken, leading to changes in the slip surface. The proposed approach does not consider these factors, leading to differences. However, the mean values of the two curves are close to each other, and combined with Specification of Seismic Design for Highway Engineering (JTG B02-2013) and Technical code for building slope engineering (GB 50330-2013), it is suggested that 0.35H-0.5H can be taken as the seismic earth pressure resultant point of gravity embankment retaining wall.

5.4 Analysis of slip surface

After the shaking-table test, the slip surface can be obtained through the connection line of the pleated deformation of the coloured sand belt on the side of the model, which is generally curved concave rather than an ideal inclined plane, as assumed in the proposed calculated approach. However, due to the limitations of the model box, the slip surface and fracture points observed in the side view are not representative, so further inference is needed to obtain a more accurate slip surface. According to the top view diagram, the backfill slides forward to form an arc, and the fracture point observed in the side view was the

contact point between the arc and the glass (point A), whereas the actual fracture point was the vertex of the arc (point B). After field measurement, the vertical distance between the two points was approximately 318 mm, as illustrated in Fig. 16. Thus, ignoring the effect of model box, the computative slip surface (this is a slip surface that occurs from the actual fracture point, also known as the actual slip surface) can be obtained by moving the observed slip surface from point A to the direction away from the wall approximately 318 mm, as depicted by the curved dotted line in Fig. 17. It can be seen that the fracture points of computative slip surface(point B) and assumed slip surface(point C) are close to each other, and the trend of computative slip surface is very close to the assumed slip surface. Thus, the theoretical slip surface assumed by the calculated approach is reasonable. Further, this indicates that the proposed method is applicable.

6. Conclusions

In this study, a simplified approach is proposed to calculate the seismic earth pressure on the EGWNS; the method has been proven to be applicable by the shaking-table test. The calculated and measured values, including those for seismic earth pressure, earth pressure resultant force, resultant force action point, and slip surface, under various PGA conditions are compared and the following conclusions are drawn:

• It can be seen that most calculated values agree well with the measured values. This indicates that the simplified approach proposed in this study is valid for calculating the seismic earth pressure on the EGWNS and provides a reliable basis for seismic design. The results of this study strictly apply to EGWNS with wall height of 1.6m, and can be assumed to be acceptable for the majority of rigid walls with cohesionless backfill.

• The calculated and measured values of seismic earth pressure increase with the increase in PGA; higher the PGA is, greater is the increase in seismic earth pressure and the difference between the calculated and measured values. Compared with the errors in calculation caused by other factors to the design of the retaining wall, the difference in between the calculation method and the measurement proposed in this study is within the allowable error range.

• The theoretical calculation of the earth pressure resultant point rises with the increase in PGA, and it is higher than the 0.33H point specified by the M-O formula. Whereas the measured point decreases with the increase in PGA, when the PGA is low, the measured resultant point is higher than the 0.33H point specified by the M-O formula; when the PGA is high, the measured resultant point approaches the 0.33H point specified by the M-O formula.

• The M-O method provides amply conservative results over the full range of accelerations, whereas the method proposed in this paper avoids overdesign while ensuring safety. In addition, the M-O formula is not applicable to high-intensity areas.

• After moving the observed slip surface approximately 318 mm away from the EGWNS, the computative slip surface can be obtained. And the fracture points of computative slip surface(point B) and assumed slip surface(point C) are close to each other, the trend of assumed slip surface is very similar to the computative slip surface. Thus, the theoretically assumed slip surface in the proposed approach is reasonable. This indicates that the proposed method is applicable.

The results of this study strictly apply to retaining structures with nonuniform slopes with wall height of 1.6m, and the relative densities of the cohesionless backfill and medium–hard soil foundation are 72% and 81%, respectively. In theory, the results of this paper can be extended to other wall heights by strict similarity law (Xu 1982). However, for the safety and economy consideration of an embankment gravity retaining wall with a nonuniform slope design, according to Technical code for building slope engineering (GB 50330-2013) and Japanese code and European code, the wall height of soil slope should not exceed 10m. So, this paper suggests that the theoretical and experimental results can be extended to the case that the wall height is 1.6m-10m. However, further research on the specific rules is needed to extend the results to the recommended wall height.

Data statement

All data, models, and code generated or used during the study appear in the submitted article.

Acknowledgments

This study was supported by the National Key R&D Program of China under Grant no. 2018YFE0207100, the National Natural Science Foundation of China under Grant no. 41602332, the Youth Scientific and Technological Innovation Team of Southwest Petroleum University under Grant no. 2018CXTD02, and the Foundation of Engineering Research Center of Eco-environment in the Three Gorges Reservoir Region of China under Grant no. KF2018-01.

References

Bolton, M.D. and Steedman, R.S. (1982), "Centrifugal testing of micro-concrete retaining walls subject to base shaking", *Proceedings of the Conference on Soil dynamics and Earthquake Engineering*, Southampton, U.K., July.

Cilingir, U., Haigh, S.K., Madabhushi, S.P.G. and Zeng, X. (2011), "Seismic behavior of anchored quay walls with dry backfill", *Geomech. Geoeng.*, **6**(3), 227-235. https://doi.org/10.1080/17486025.2011.578670.

Chowdhury, I. and Singh, J.P. (2015), "Behavior of gravity type retaining wall under earthquake load with generalized backfill", *J. Earthq. Eng.*, **19**(4), 563-591. https:// doi.org/10.1080/13632469.2014.997900.

Choudhury, D. and Nimbalkar, S. (2007), "Seismic rotational displacement of gravity walls by pseudo-dynamic method: Passive case", *Soil Dyn. Earthq. Eng.*, **27**(3), 242-249. https://doi.org/10.1016/j.soildyn.2006.06.009.

Evans and John, H. (1972), "Dimensional Analysis and the Buckingham Pi Theorem", *Am. J. Phys.*, **40**(12), 1815-1822. https://doi.org/10.1119/1.1987069.

Eurocode 8 (1988), Design of structures for earthquake resistance, Part 5: Foundations, retaining structures and geotechnical aspects.

Harris, H.G. (1982), Dynamic Modeling of Concrete Structure. Publication SP-73, ACI, Detroit, U.S.A.

Ishibashi, I. and Fang, Y.S. (1987), "Dynamic earth pressures with different wall movement modes", *Soils. Found.*, **4**(27), 11-22. https://doi.org/10.3208/sandf1972.27.4_11.

Jo, S.B., Ha, J.G. and Lee, J.S. (2017), "Evaluation of the seismic earth pressure for inverted T-shape stiff retaining wall in cohesionless soils via dynamic centrifuge", *Soil Dyn. Earthq. Eng.*, **92**, 345-357. https://doi.org/10.1016/j.soildyn.2016.10.009.

Jesmani, M., Kamalzare, M. and Sarbandi, B.B. (2016), "Seismic response of geosynthetic reinforced retaining walls", *Geomech. Eng.*, **10**(5), 635-655. https://doi.org/10.12989/gae.2016.10.5.635.

Japan Railway Integrated Technology Research Institute (1998), Japan Railway Structure Design Standard.

Kagawa, T., Sato, M., Minowa, C., Abe, A. and Tazoh, T. (2004), "Centrifuge simulations of large-scale shaking table tests: Case studies", *J. Geotech. Geoenviron. Eng.*, **130**(7), 663-672. https://doi.org/10.1061/(ASCE)1090-0241(2004)130:7(663).

GB 50330-2013 (2013), Technical code for building slope engineering, Ministry of Housing and Urban-Rural Development of the People's Republic of China, Beijing, China.

Matsuo, H. (1941), "Experimental study on the distribution of Earth pressures acting on a vertical wall during earthquakes", *J. Jpn. Soc. Civ. Eng..*, **2**(27), 83-106.

Mononobe, N. and Matsuo, M. (1929), "On the determination of Earth pressures during earthquakes", *Proceedings of the World Engineering Congress*, Tokyo, Japan.

Mylonakis, G., Kloukinas, P. and Papatonopoulos, C. (2007), "An Alternative to the Mononobe-Okabe Equation for Seismic Earth Pressures", *Soil Dyn. Earthq. Eng.*, **10**(27), 957-969. https://doi.org/10.1016/j.soildyn.2007.01.004.

Ma, D.F., Guo, L. and Wu, J.Q. and Zhou, Z.D. (2014), "Comparative analysis on different types of anchor reinforcing gravity retaining wall", *Appl. Mech. Mater.*, **477-478**, 567-571. https://doi.org/10.4028/www.scientific.net/AMM.477-478.567.

Mikola, R.G., Candia, G.A. and Sitar, N. (2016), "Seismic Earth pressures on retaining structures and basement walls in cohesionless soils", *J. Geotech. Geoenviron. Eng.*, **142**(10), 04016047(1-9). https://doi.org/10.1061/(ASCE)GT.1943-5606.0001507.

Okabe, S. (1926), "General theory of Earth pressure", *J. Jpn. Soc. Civ. Eng.*, **1**(12).

Qu, H.L., Li, R.F., Hu, H.G., Jia, H.Y. and Zhang, J.J. (2016), "An approach of seismic design for sheet pile retaining wall based on capacity spectrum method", *Geomech. Eng.*, **11**(2), 309-323. https://doi.org/10.12989/gae.2016.11.2.309.

Qu, H.L., Luo, H., Hu, H.G., Jia, H.Y. and Zhang, D.Y. (2018), "Dynamic response of anchored sheet pile wall under ground motion: Analytical model with experimental validation", *Soil Dyn. Earthq. Eng.*, **115**, 896-906. https://doi.org/10.1016/j.soildyn.2017.09.015.

Steedman, R.S. and Zeng, X. (1990), "The influence of phase on the calculation of pseudo-static earth pressure on a retaining wall", *Geotechnique*, **40**(1), 103-112. https://doi.org/10.1680/geot.1990.40.1.103.

Sitar, N., Mikola, R.G. and Candia, G.A. (2012), "Seismically induced lateral earth pressures on retaining structures and basement walls", *Proceedings of the GeoCongress 2012,* Oakland, California, U.S.A., March.

Sherif, M.A., lshibashi, I. and Lee, C.D. (1982), "IL Earth pressure against rigid retaining wall", *J. Geotech. Eng.*, **108**(5), 679-695. https://10.1016/0022-1694(82)90165-2.

Santhoshkumar, G. and Ghosh, P. (2018), "Seismic passive earth pressure on an inclined cantilever retaining wall using method of stress characteristics - A new approach", *Soil. Dyn. Earthq. Eng.*, **107**, 77-82. https://10.1016/j.soildyn.2018.01.021.

Wagner, N. and Sitar, N. (2018), "Comparison of pseudo-static limit equilibrium and elastic wave equation analyses of dynamic Earth pressures on retaining structures", *Proceedings of the 5th Geotechnical Earthquake Engineering and Soil Dynamics Conference*, Austin, Texas, U.S.A., June.

Xu, P., Hatami, K. and Jiang, G.L. (2020), "Study on seismic stability and performance of reinforced soil walls using shaking table tests", *Geotext. Geomembranes*, **48**(1), 82-97. https://doi.org/10.1016/j.geotexmem.2019.103507.

Xu, T. (1982), *Similarity Theory and Model Test,* China Agricultural Machinery Press, Beijing, China.

Yang, X.L., and Li, Z.W. (2018), "Upper bound analysis of 3D static and seismic active earth pressure", *Soil. Dyn. Earthq. Eng.*, **108**, 18-28.

https://108,18-28. 10.1016/j.soildyn.2018.02.006.

Zhang, J., Qu H.L., Liao, Y. and Ma, Y.X. (2012), "Seismic damage of earth structures of road engineering in the 2008 Wenchuan earthquake", *Environ. Earth Sci.*, **65**, 987-993. https://doi.org/10.1007/s12665-011-1519-5.

Zhang, H.B., Zheng, L.Z., Song, X.G. and Xu, J.P. (2011), "Research on the supporting mechanism of gravity retaining wall with grouting anchor in high filling embankment", *Adv. Civ. Eng.*, **90-93**, 514-517. https://doi.org/10.4028/www.scientific.net/amm.90-93.514.

IC